Electronic Supplementary Material for Organic & Biomolecular Chemistry

Copper(II)-Mediated Resolution of *α*-Halo Carboxylic Acids with Chiral *O,O*'-Dibenzoyltartaric Acid: Spontaneous Racemisation and Crystallization-Induced Dynamic Resolution

Hong-wu Xu[ac], Qi-wei Wang[a], Jin Zhu[ac], Jin-gen Deng*[ac], Lin-feng Cun[a], Xin Cui[a], Jun Wu[a], Xin-liang Xu[b], Yu-liang Wu[b]

[a] *Key Laboratory of Asymmetric Synthesis & Chirotechnology of Sichuan Province and Union Laboratory of Asymmetric Synthesis, Chengdu Institute of Organic Chemistry, Chinese Academy of Sciences, Chengdu 610041, China. E-mail: jgdeng@cioc.ac.cn.*
[b] *Zhejiang APELOA Medical Technology Co. Ltd., Dongyang 322118, China.*
[c] *Graduate School of the Chinese Academy of Sciences, Beijing 100039, China.*

1. Resolution of HL^1 in $EtOH/H_2O$

Syntheses of $Cu_2(L^0)(L^1)(OAc)(H_2O)_2$ (Complex 10): To a solution of *D*-DBTA·H_2O (760 mg, 0.2 mmol) and racemic *α*-bromo-2-chlorophenylacetic acid (1.0 g, 0.2 mmol) in 5 mL of EtOH/H_2O (3:1) was added $Cu(OAc)_2·H_2O$ (800 mg, 0.4 mmol). After stirred for 12 hours, the mixture was cooled to -10°C overnight. The resulted green precipitate was filtered, washed with 10 mL of EtOH and air-dried at room temperature. Yield: 21.3% (based on the racemic acid). Anal. ($C_{28}H_{24}O_{14}ClBrCu_2$) C, H, N, Cu: calcd, 40.67%, 2.93%, 0, 15.4%; found, 40.54%, 3.03%, 0, 15.2%. IR absortion bands (cm^{-1}): 3455 (br), 3063 (w), 1716 (s), 1651 (vs), 1602 (vs), 1400 (s), 1267 (s), 1177 (w), 1114 (m), 1070 (w), 1026 (w), 741 (m), 711 (m). UV-Vis of the solid sample (λ/nm): 365, 690.

Optically active (*S*)-*α*-bromo-2-cholophenylacetic acid was obtained after decomposition of the complex. Yield: 20.2% (based on the racemic acid). Ee: 25.7 %; ^1H NMR (300 MHz, $CDCl_3$), *δ*: 10.43 (br, 1H, COOH), 7.05-7.70 (m, 4H, Ar-H), 5.74 (s, 1H, CH) ppm.

2. Determination of enantiomeric excess of the acids.

2.1 Enantiomeric excess of HL^1 to HL^5 were determined by HPLC analysis on chiral column (Chiralcel AS), heptane-2-propanol-trifluoroacetic acid (90:10:0.1), flow rate: 1.0 mL/min.

Retention times for HL^1: 6.0 and 7.3 min.

Retention times for HL^2: 6.0 and 6.9 min.

Retention times for HL^3: 6.2 and 7.5 min.

Retention times for HL^4: 5.8 and 7.3 min.

Retention times for HL^5: 6.1 and 7.0 min.

2.2 The enantiomeric excess of HL^6 and HL^7 were determined by GC analysis on chiral column (Chiralcel Dex 225 column, 155°C, 12 psi) after conversion to the corresponding ethyl esters.

Retention times for *α*-bromophenylacetic acid ethyl ester: 5.90 and 6.17 min.

Retention times for *α*-Bromo-4-chlorophenylacetic acid ethyl ester: 8.57 and 9.17 min.

2.3 The enantiomeric excess HL^8 and HL^9 were also determined by GC analysis on chiral column

(Chiralcel Dex column, 100°C, 10 psi) after conversion to the corresponding ethyl esters.

Retention times for 2-bromopropionic acid ethyl ester: 1.84 and 1.91 min.

Retention times for 2-chloropropionic acid ethyl ester: 1.80 and 1.86 min.

3. Determination of the reaction time

To a solution of *D*-DBTA·H_2O (760 mg, 0.2 mmol) and racemic α-bromo-2-chlorophenylacetic acid (HL^1, 1.0 g, 0.4 mmol) in 10 mL of acetonitrile at 40°C was added $Cu(OAc)_2 \cdot H_2O$ (800 mg, 0.4 mmol). After stirred for about five minutes, $Cu(OAc)_2$ was dissolved and the mixture became clear. Two days later, green precipitate formed. The diastereomic excess of the complex was monitored and determined based on HL^1 obtained after decomposition of the complex. The results showed the best enantioselectivity was obtained when the reaction time was 7 days (Fig. 1).

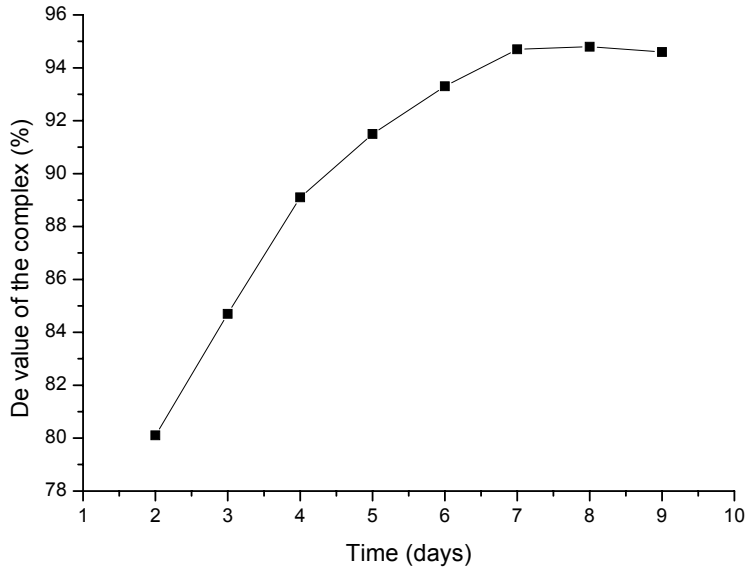

Fig. 1

4. **The IR spectra**

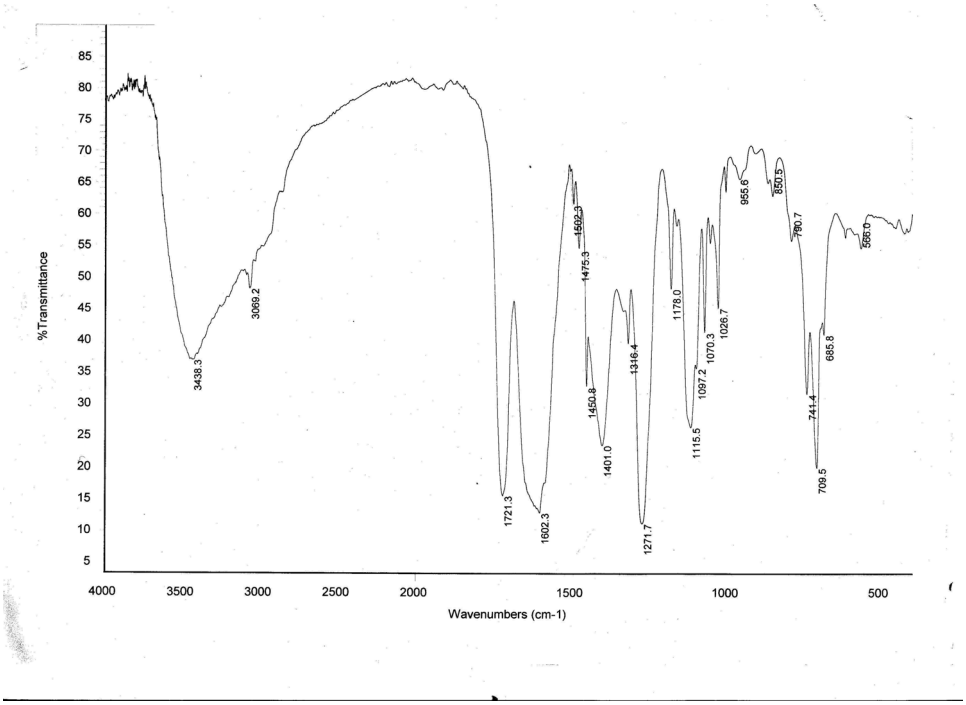

Fig. The IR spectrum of $[Cu_2(L^0)(L^1)(OAc)(H_2O)_2]\cdot 1.5MeCN$ (Complex 1).

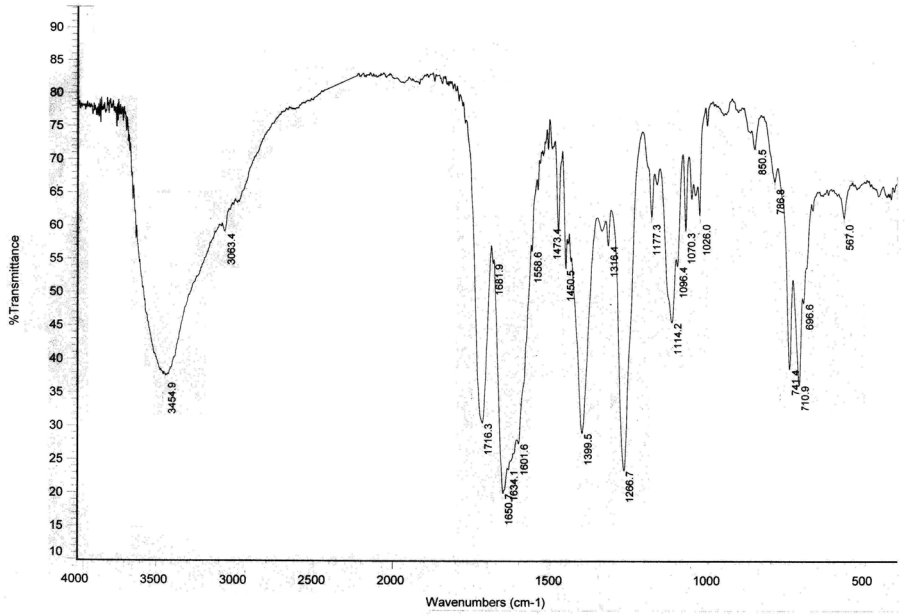

Fig. The IR spectrum of $Cu_2(L^0)(L^1)(OAc)(H_2O)_2$ (Complex 10).

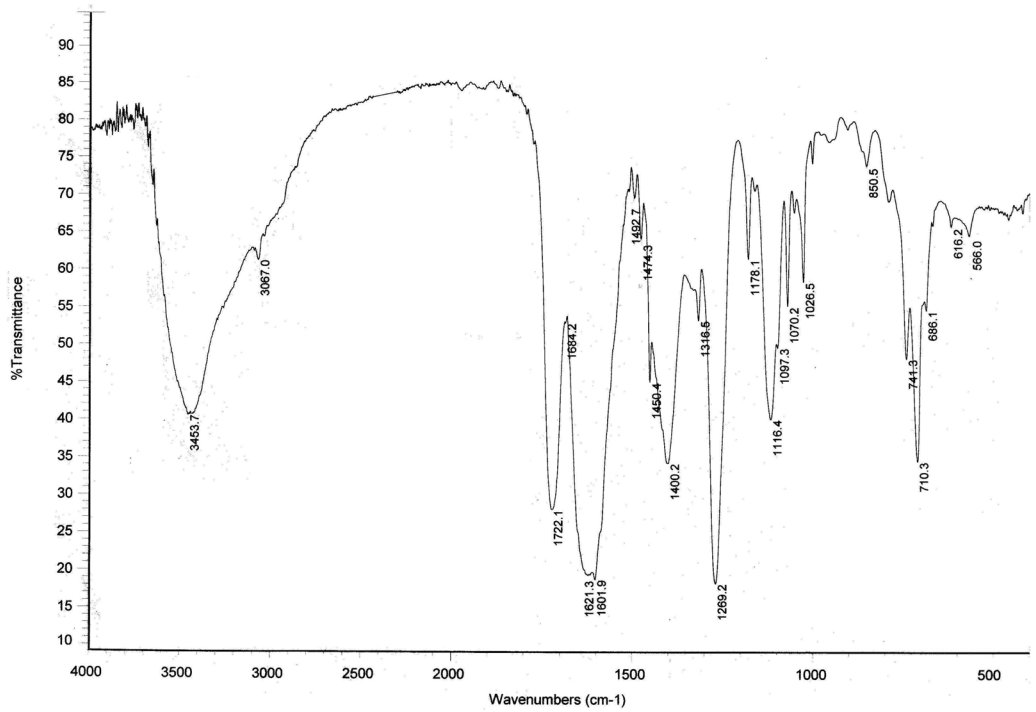

Fig. The IR spectrum of the solid complex 1 (dried in vacuum for five hours at 50°C).

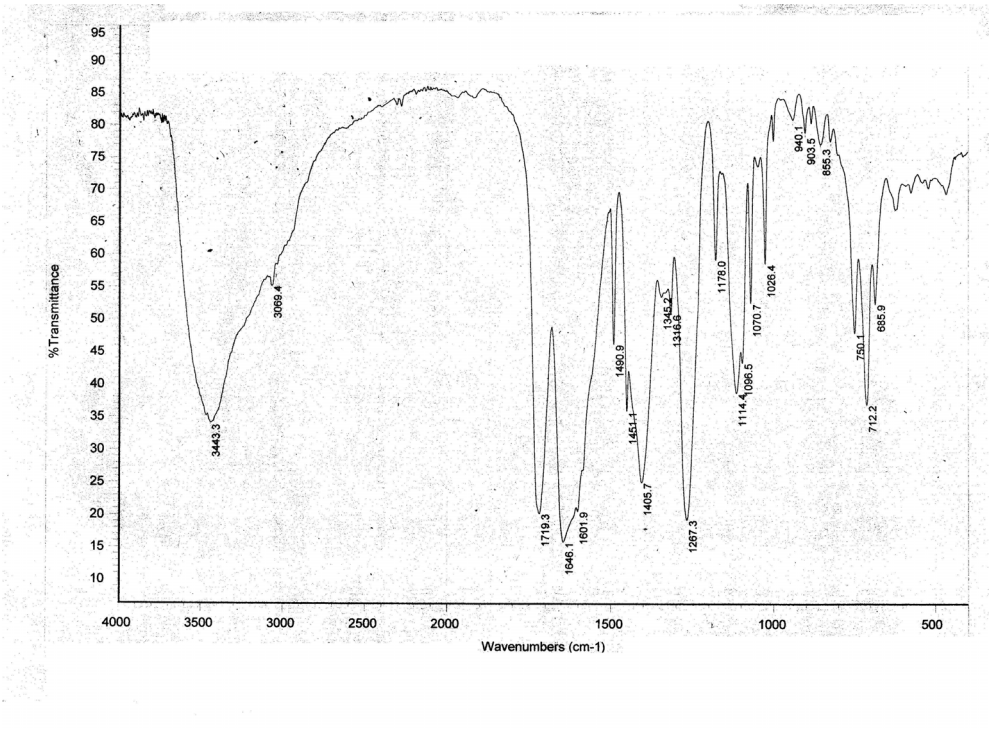

Fig. The IR spectrum of $[Cu_2(L^0)(L^2)(OAc)(H_2O)_2]\cdot 1.5MeCN$ (Complex 2).

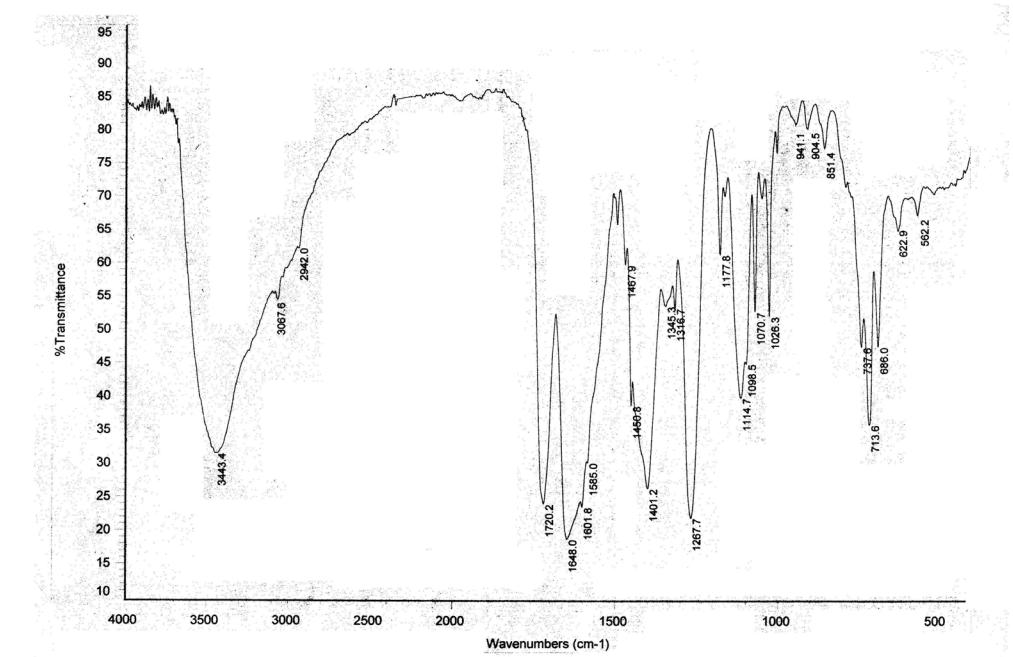

Fig. The IR spectrum of $[Cu_2(L^0)(L^3)(OAc)(H_2O)_2]\cdot 2MeCN$ (Complex 3).

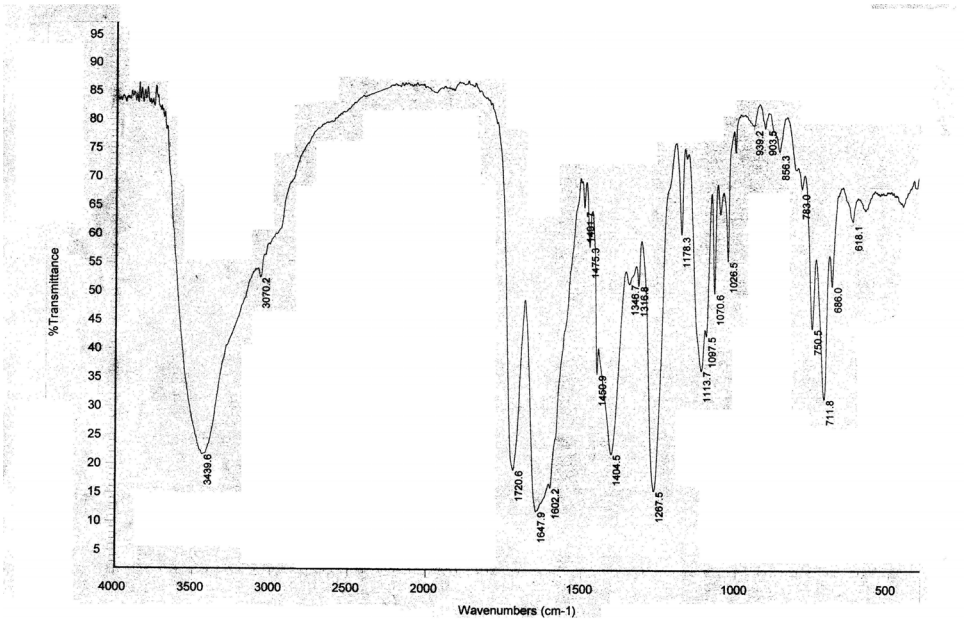

Fig. The IR spectrum of $[Cu_2(L^0)(L^4)(OAc)(H_2O)_2]\cdot 1.5MeCN$ (Complex 4).

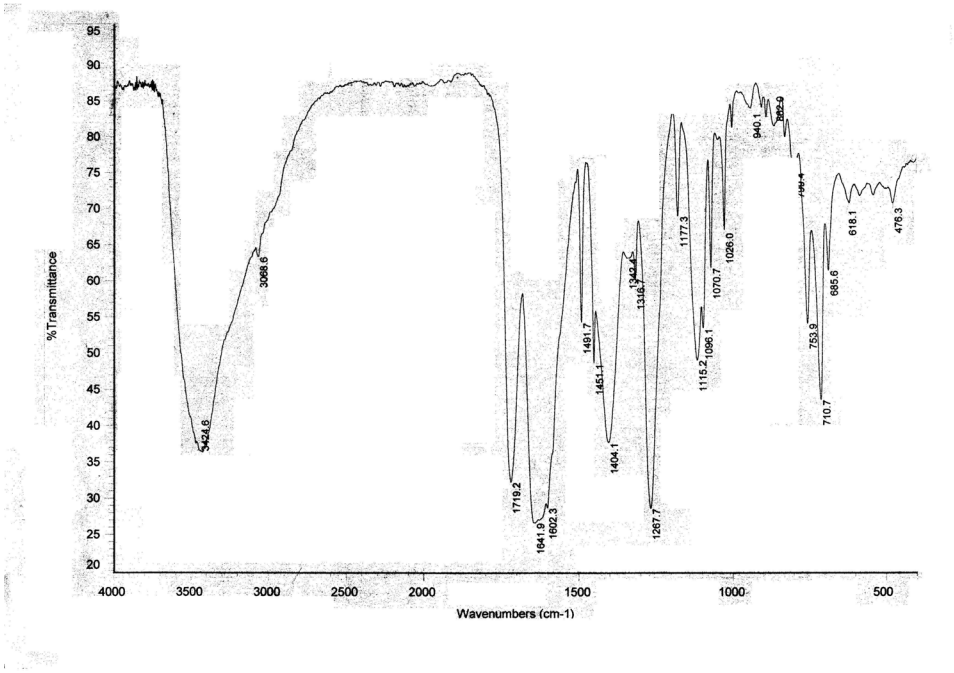

Fig. The IR spectrum of $[Cu_2(L^0)(L^5)(OAc)(H_2O)_2]\cdot 1.5MeCN$ (Complex 5).

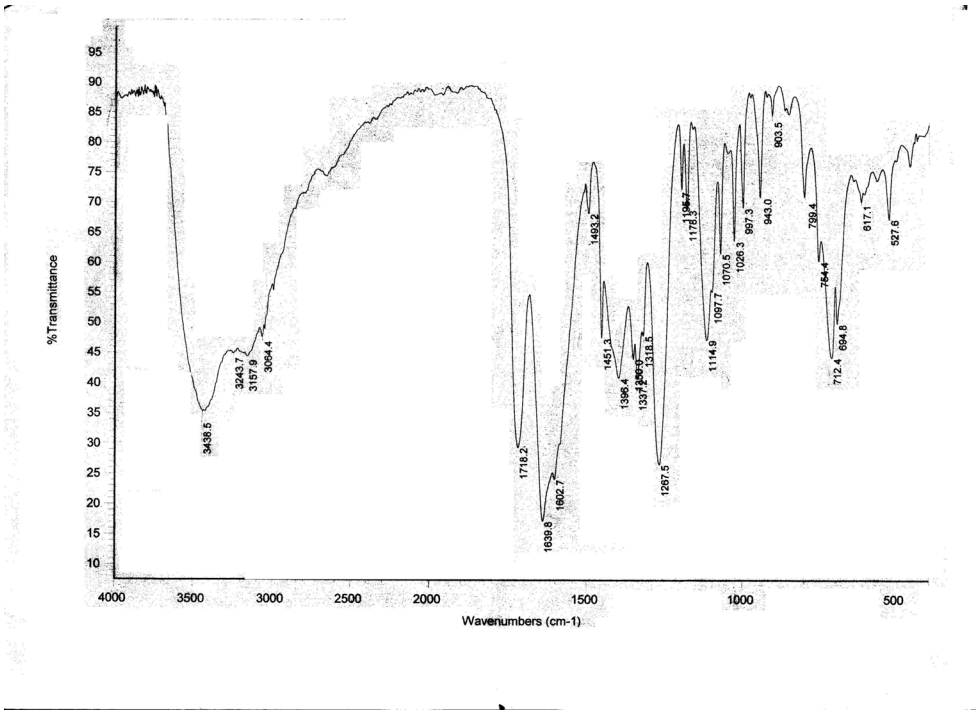

Fig. The IR spectrum of $Cu(HL^0)(L^6)(H_2O)_{1.5}$ (Complex 6).

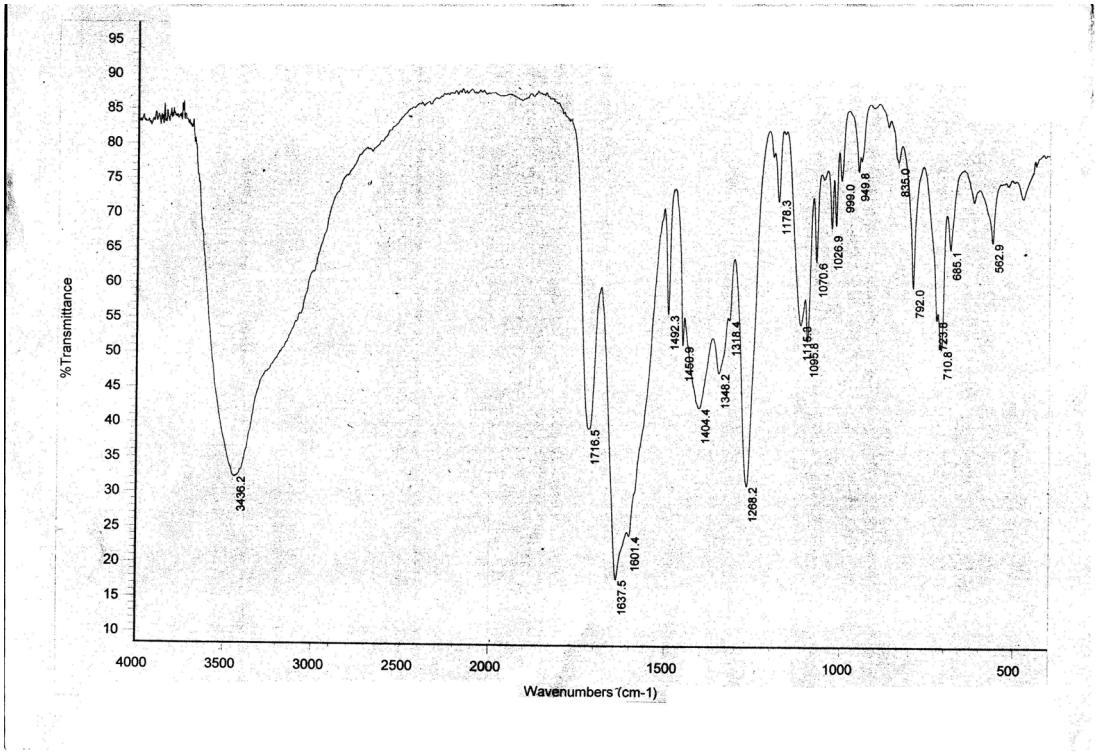

Fig. The IR spectrum of $Cu_2(L^0)(L^7)(OAc)(H_2O)_2$ (Complex 7).

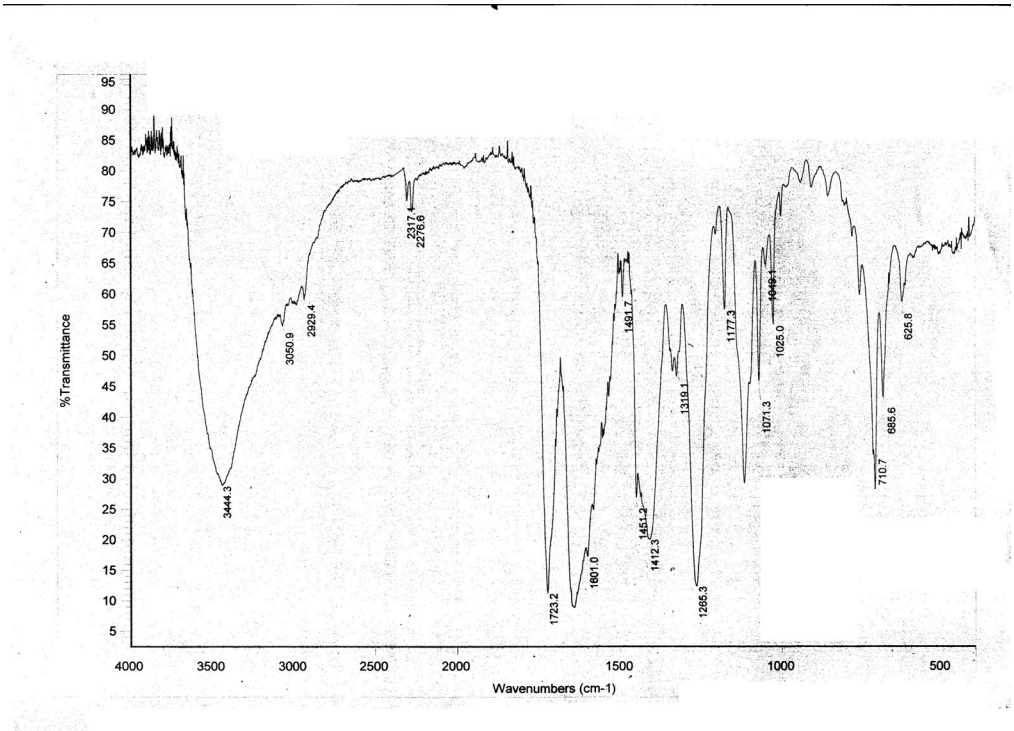

Fig. The IR spectrum of $[Cu_2(L^0)(L^8)(OAc)(H_2O)_2] \cdot 1.5MeCN$ (Complex 8).

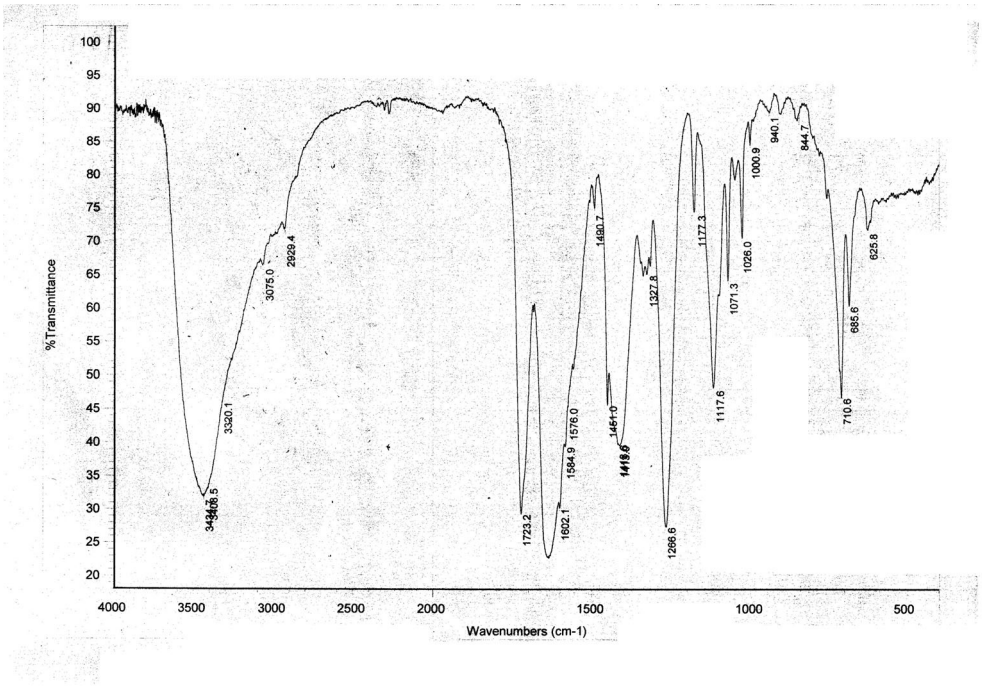

Fig. The IR spectrum of $[Cu_2(L^0)(L^9)(OAc)(H_2O)_2]\cdot 1.5MeCN$ (Complex 9).

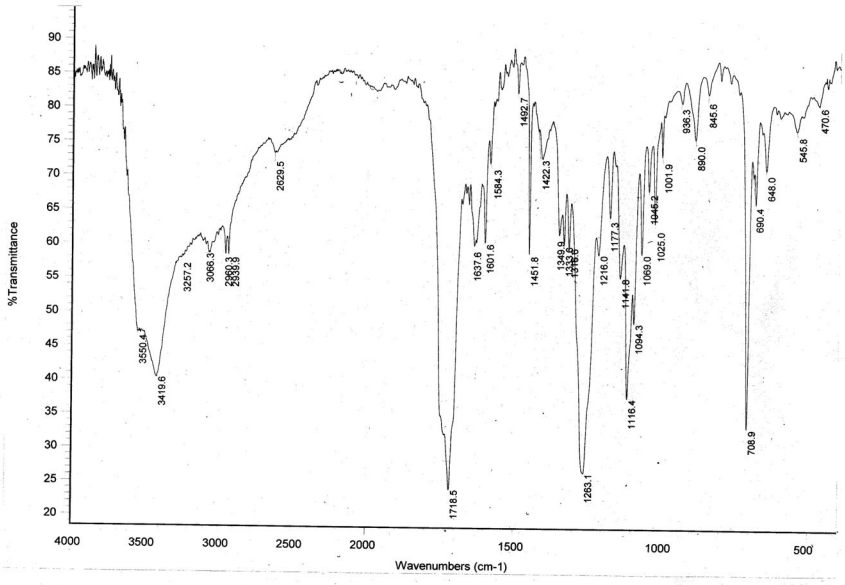

Fig. The IR spectrum of DBTA.

5. The UV-vis spectra of the solid complexes

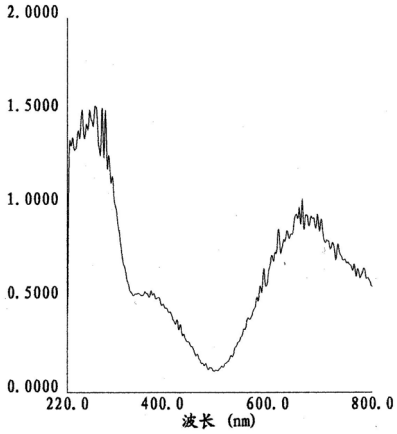

Fig. The UV-vis spectrum of $[Cu_2(L^0)(L^1)(OAc)(H_2O)_2]\cdot 1.5MeCN$ (Complex 1).

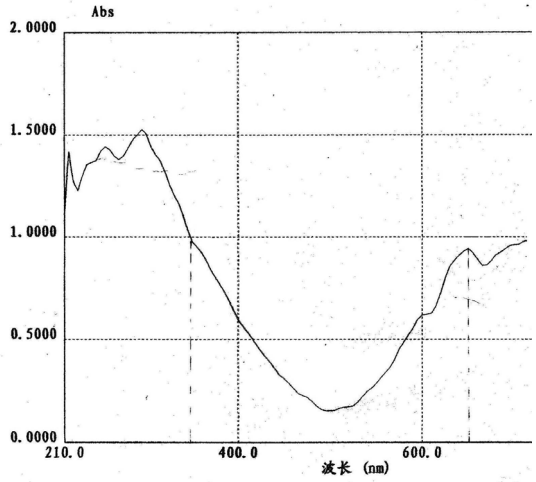

Fig. The UV-vis spectrum of $Cu_2(L^0)(L^1)(OAc)(H_2O)_2$ (Complex 10).

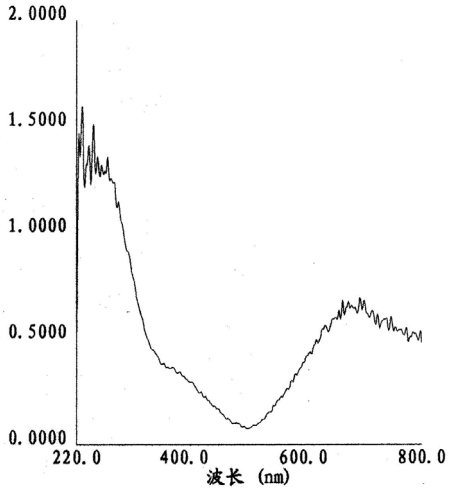

Fig. The UV-vis spectrum of $[Cu_2(L^0)(L^2)(OAc)(H_2O)_2]\cdot 1.5MeCN$ (Complex 2).

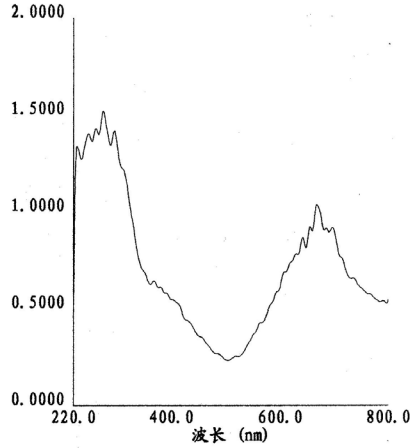

Fig. The UV-vis spectrum of $[Cu_2(L^0)(L^3)(OAc)(H_2O)_2]\cdot 2MeCN$ (Complex 3).

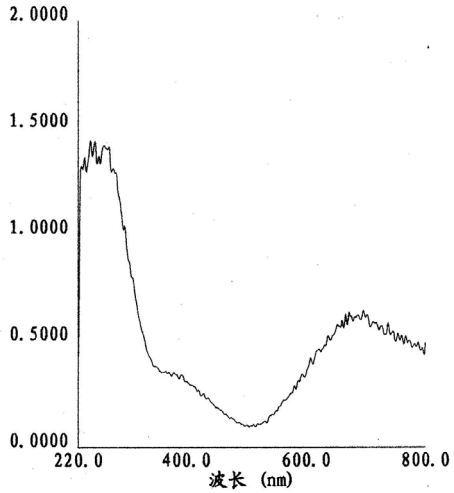

Fig. The UV-vis spectrum of $[Cu_2(L^0)(L^4)(OAc)(H_2O)_2]\cdot 1.5MeCN$ (Complex 4).

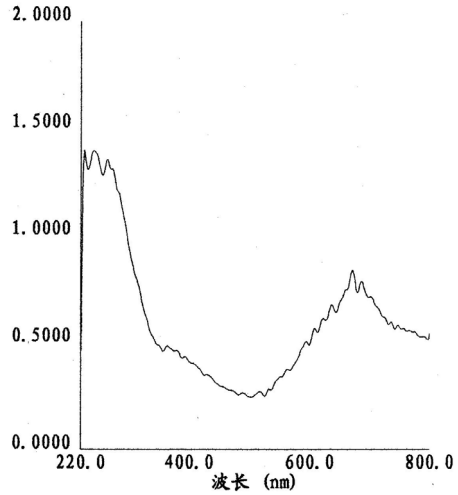

Fig. The UV-vis spectrum of $[Cu_2(L^0)(L^5)(OAc)(H_2O)_2]\cdot 1.5MeCN$ (Complex 5).

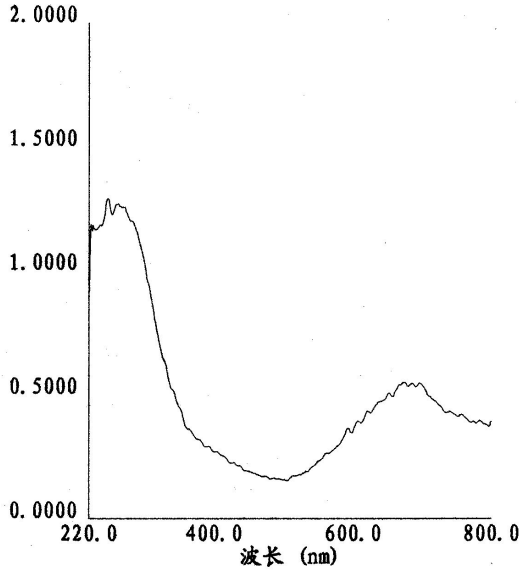

Fig. The UV-vis spectrum of $Cu(HL^0)(L^6)(H_2O)_{1.5}$ (Complex 6).

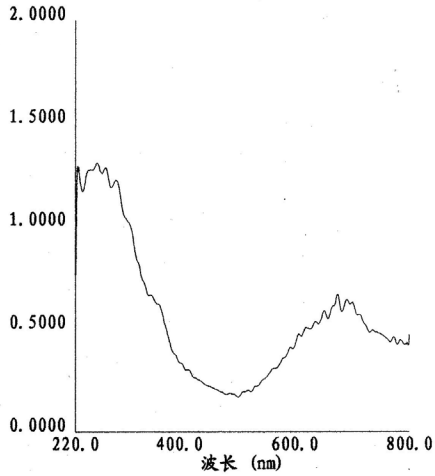

Fig. The UV-vis spectrum of $Cu_2(L^0)(L^7)(OAc)(H_2O)_2$ (Complex 7).

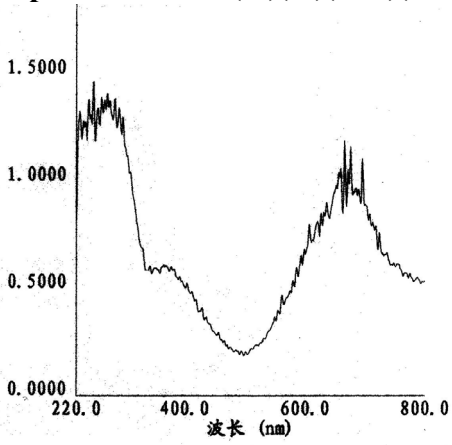

Fig. The UV-vis spectrum of $[Cu_2(L^0)(L^8)(OAc)(H_2O)_2]\cdot 1.5MeCN$ (Complex 8).

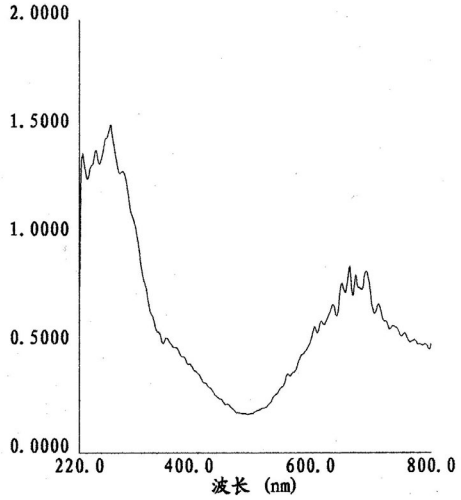

Fig. The UV-vis spectrum of $[Cu_2(L^0)(L^9)(OAc)(H_2O)_2]\cdot 1.5MeCN$ (Complex 9).

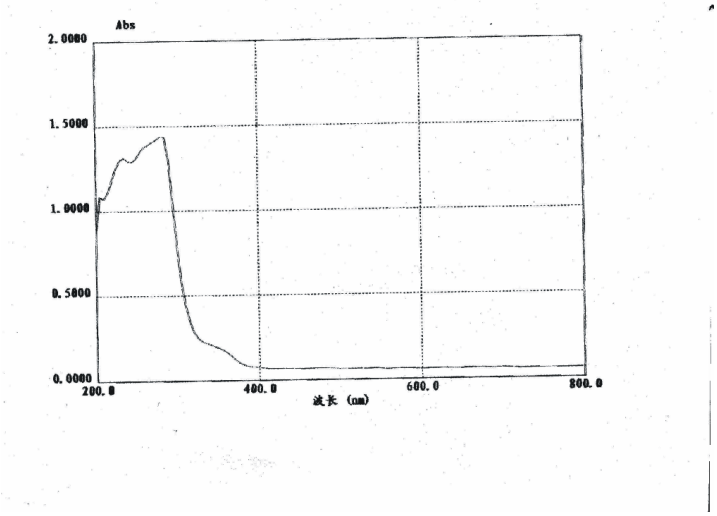

Fig. The UV-vis spectrum of DBTA.

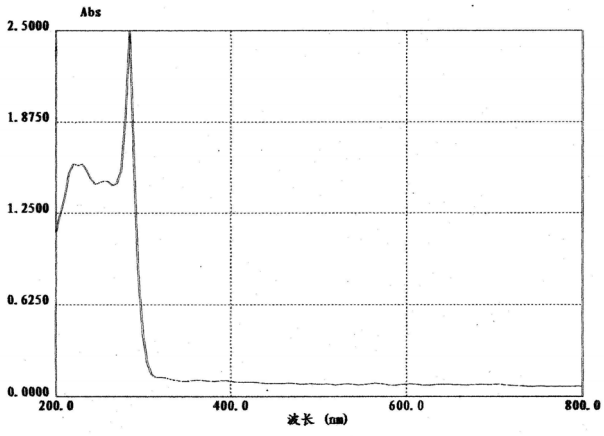

Fig. The UV-vis spectrum of HL^1.

6. TGA chart

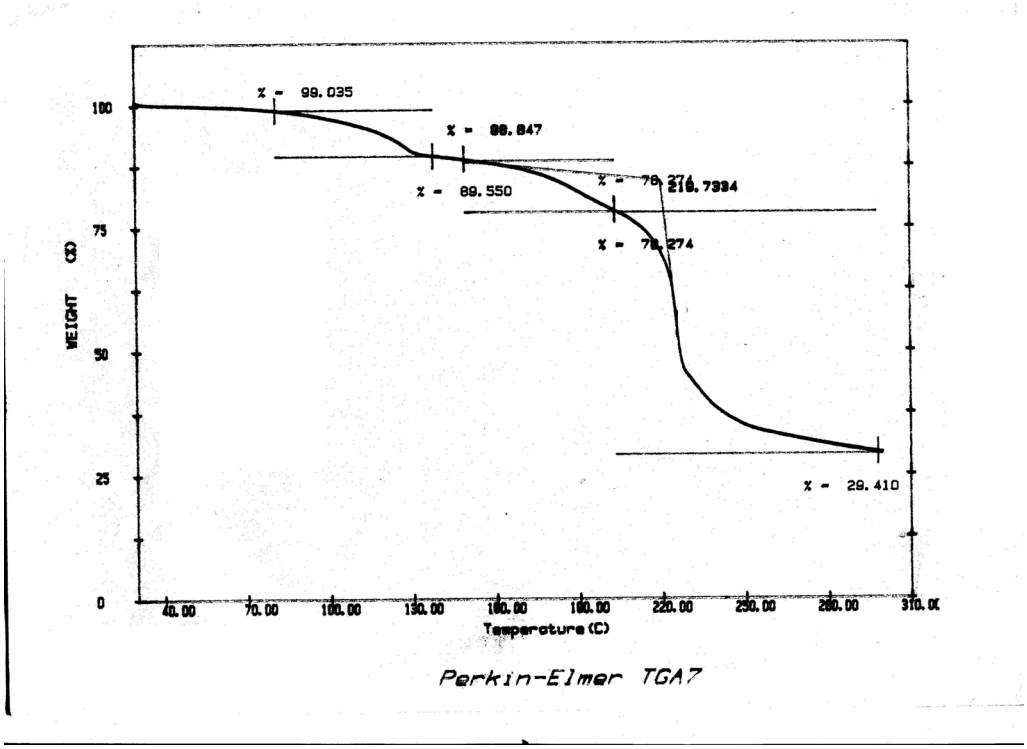

Fig. The thermogram of $[Cu_2(L^0)(L^1)(OAc)(H_2O)_2]\cdot 1.5MeCN$ (Complex 1).

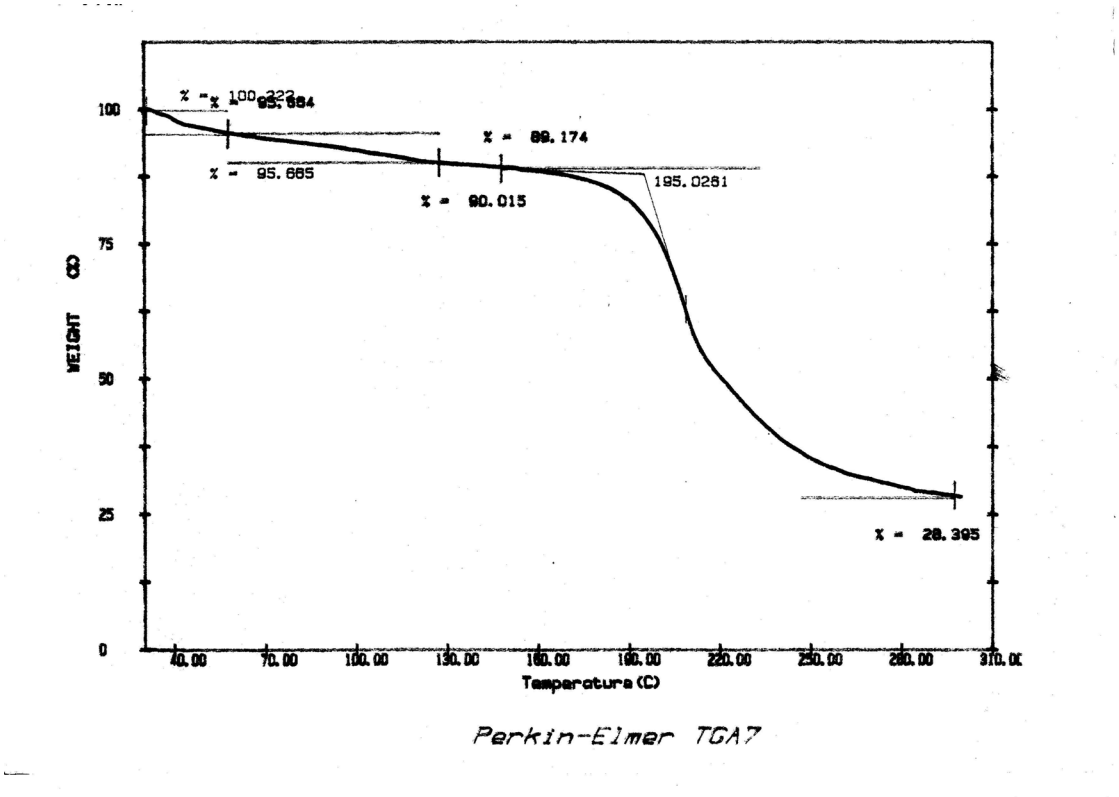

Fig. The thermogram of $Cu_2(L^0)(L^1)(OAc)(H_2O)_2$ (Complex 10).

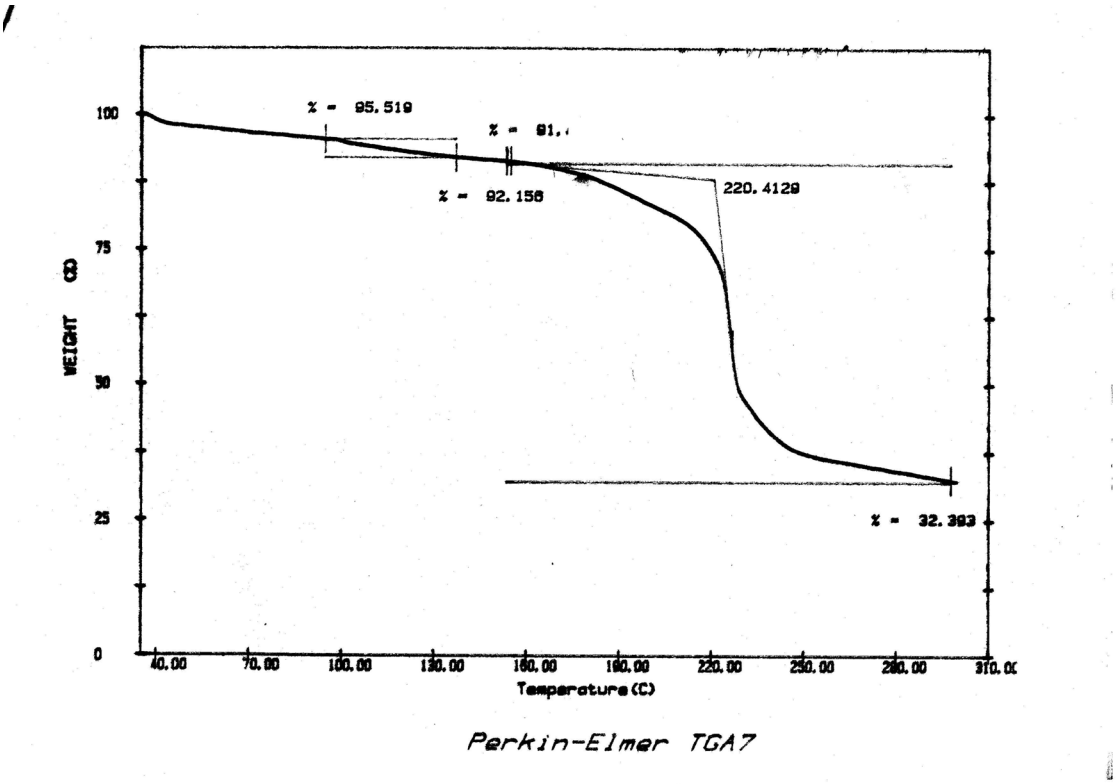

Fig. The thermogram of the solid complex 1 (dried in vacuum for five hours at 50°C).

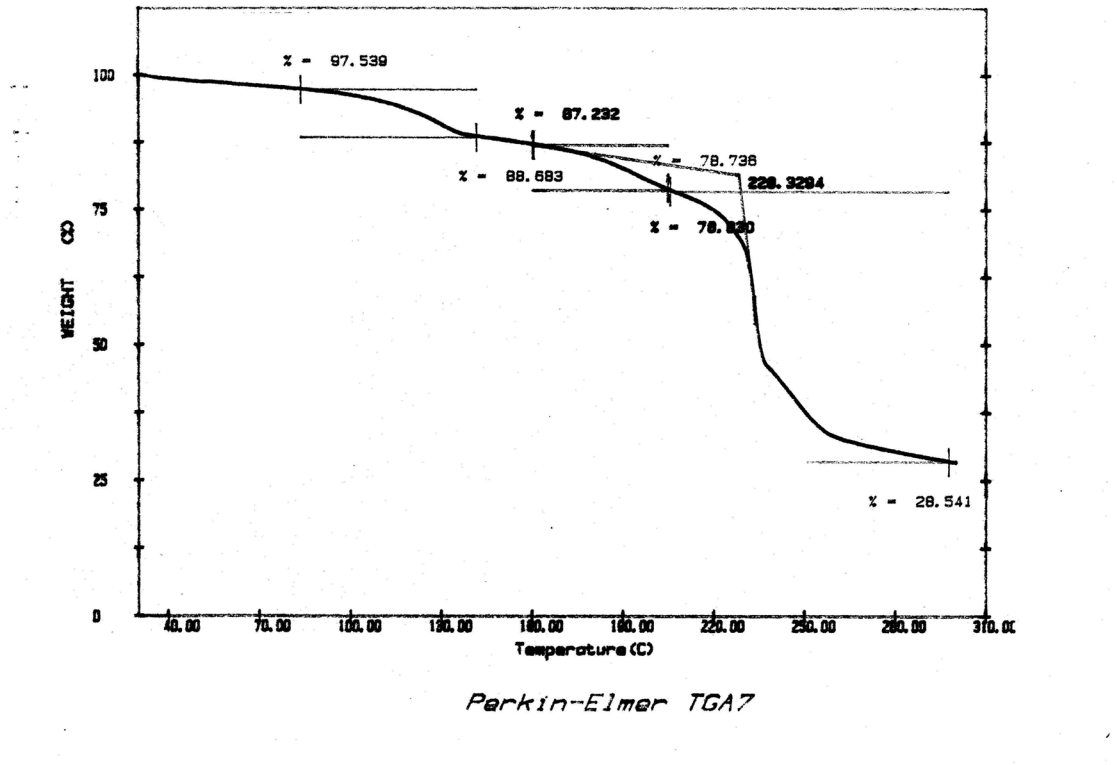

Fig. The thermogram of $[Cu_2(L^0)(L^2)(OAc)(H_2O)_2]\cdot 1.5MeCN$ (Complex 2).

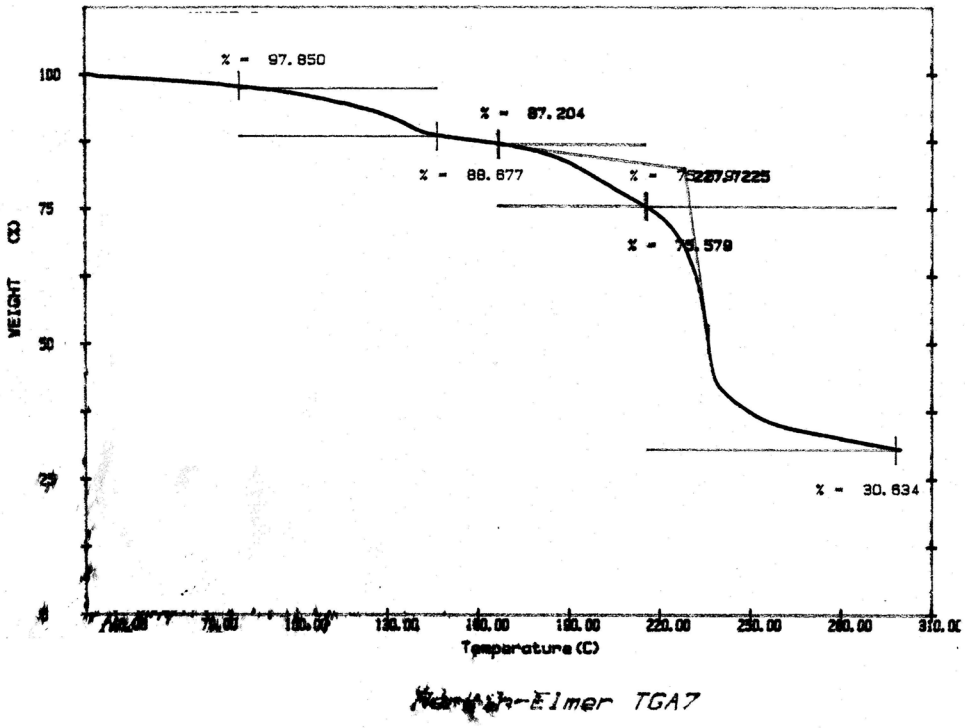

Fig. The thermogram of $[Cu_2(L^0)(L^3)(OAc)(H_2O)_2]\cdot 2MeCN$ (Complex 3).

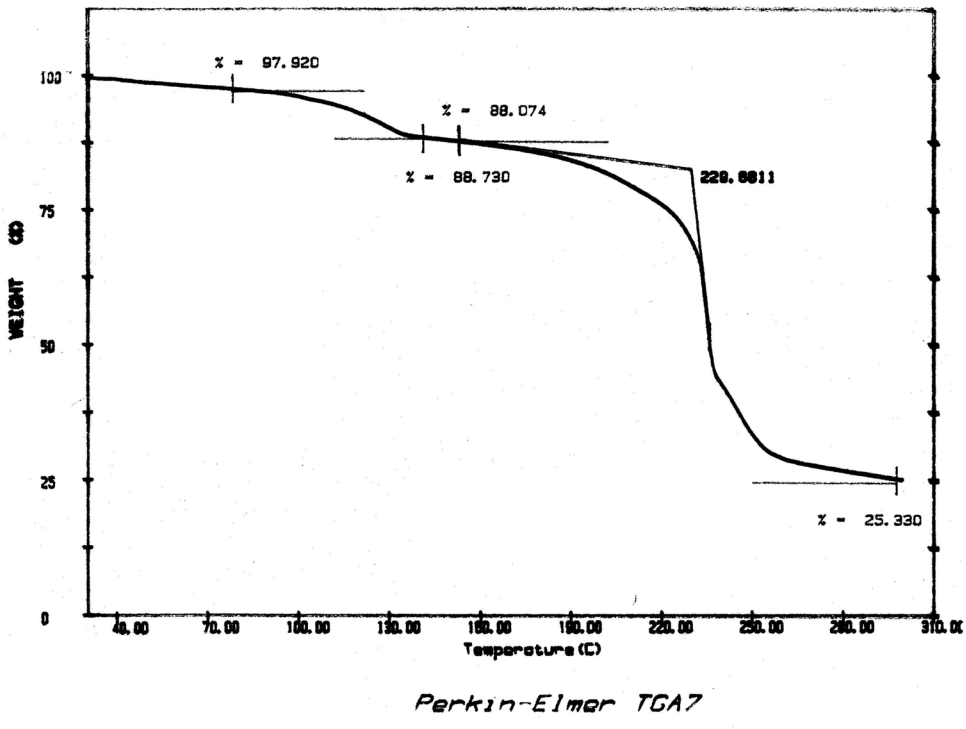

Fig. The thermogram of $[Cu_2(L^0)(L^4)(OAc)(H_2O)_2]\cdot 1.5MeCN$ (Complex 4).

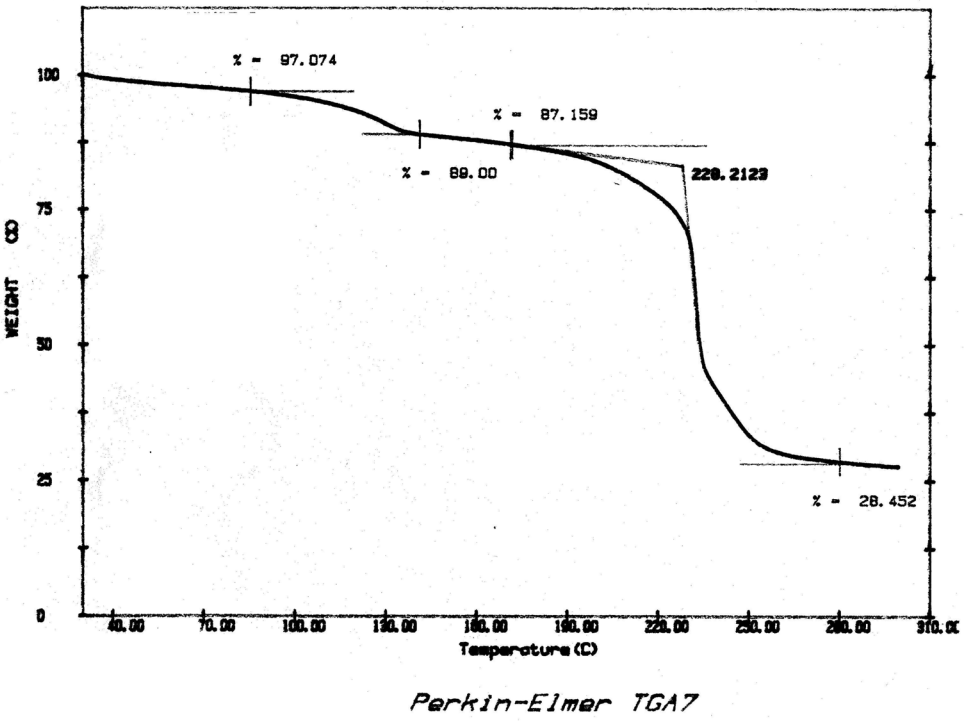

Fig. The thermogram of $[Cu_2(L^0)(L^5)(OAc)(H_2O)_2]\cdot 1.5MeCN$ (Complex 5).

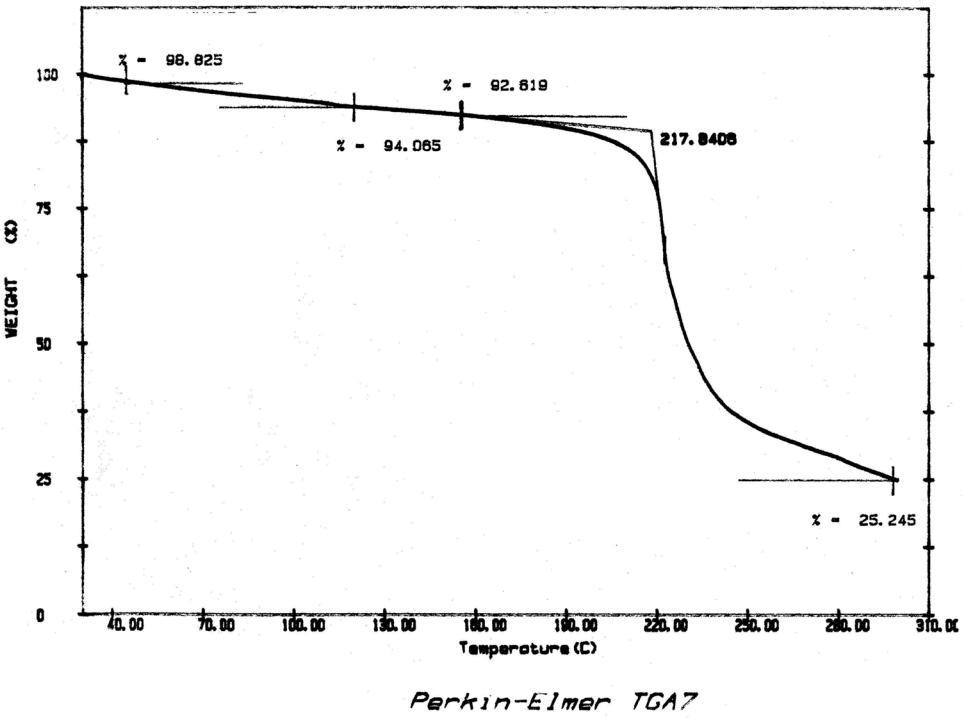

Fig. The thermogram of $Cu(HL^0)(L^6)(H_2O)_{1.5}$ (Complex 6).

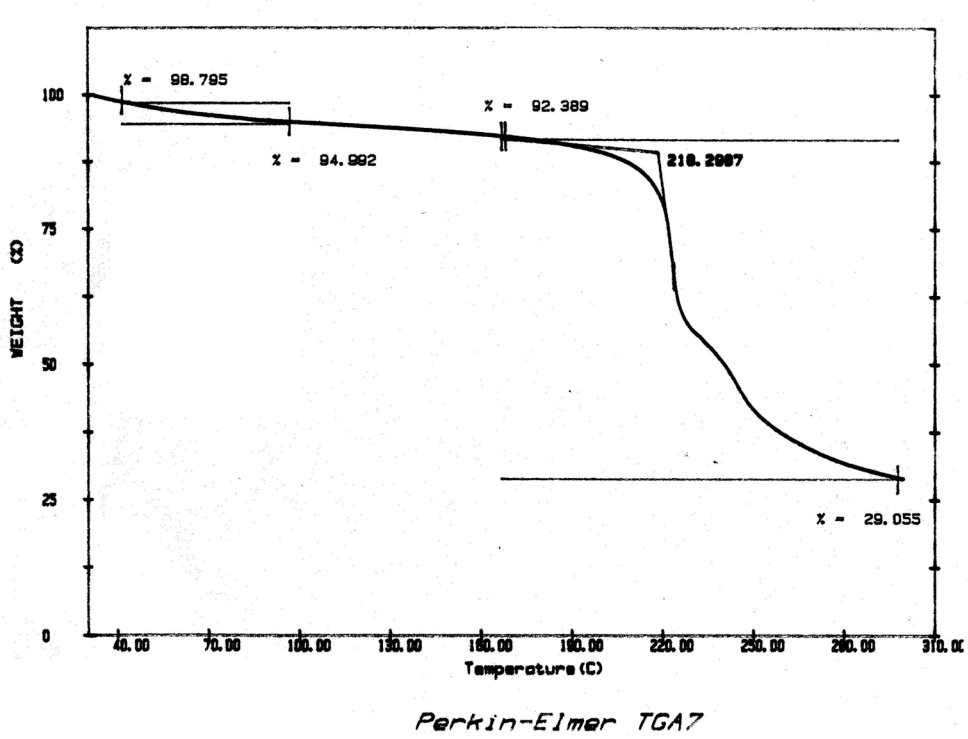

Fig. The thermogram of $Cu_2(L^0)(L^7)(OAc)(H_2O)_2$ (Complex 7).

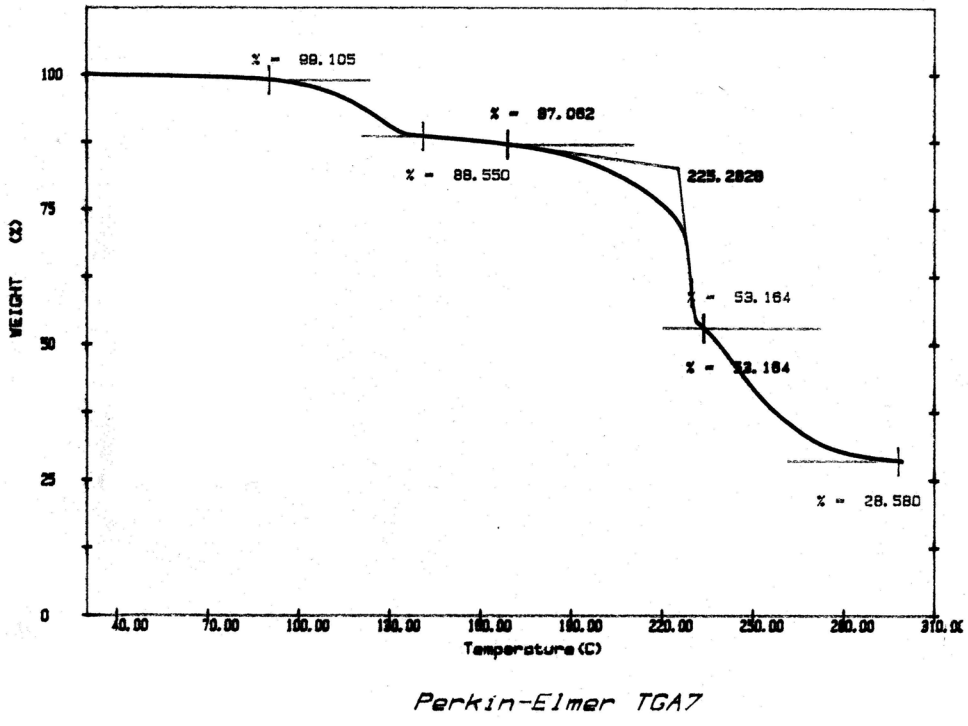

Fig. The thermogram of $[Cu_2(L^0)(L^8)(OAc)(H_2O)_2] \cdot 1.5MeCN$ (Complex 8).

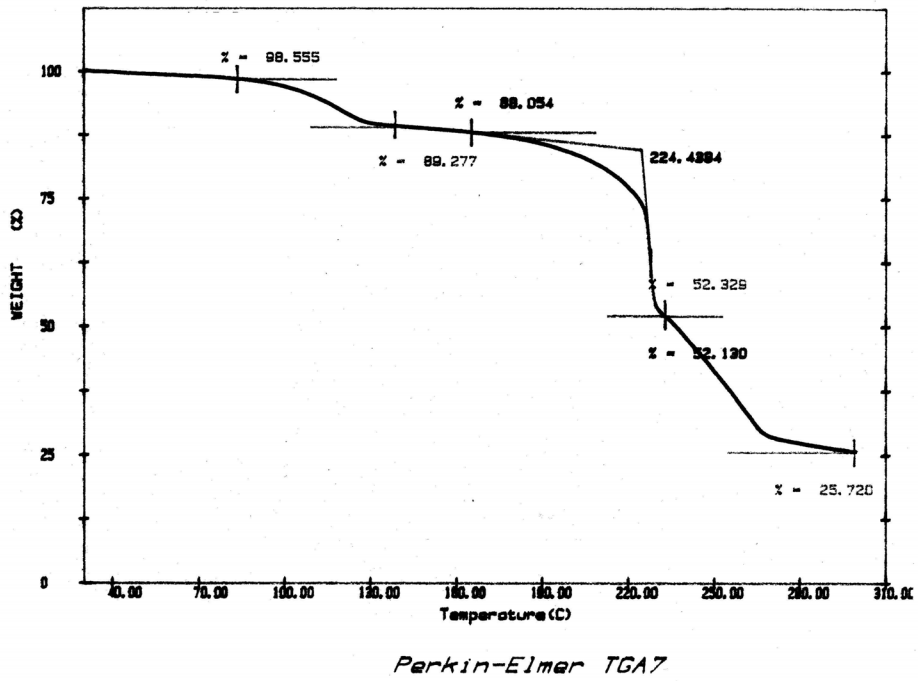

Fig. The thermogram of $[Cu_2(L^0)(L^9)(OAc)(H_2O)_2]\cdot 1.5MeCN$ (Complex 9).

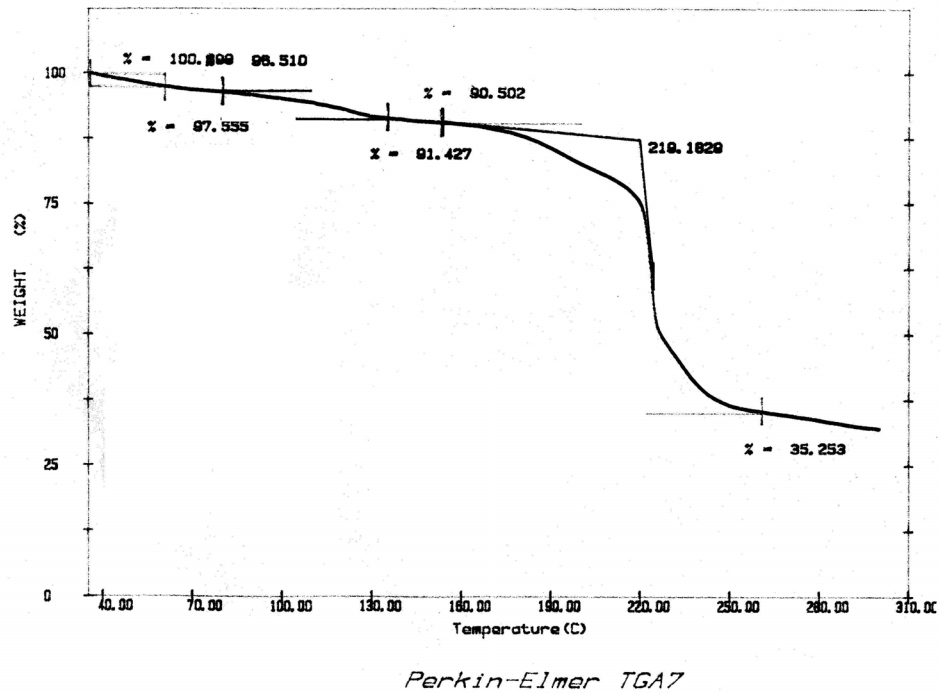

Fig. The thermogram of the complex (obtained from reaction of (*R*)-HL[1] with 93.6% ee, *D*-DBTA·H_2O and $Cu(OAc)_2\cdot H_2O$ (1:1:2 molar ratio) in acetonitrile).

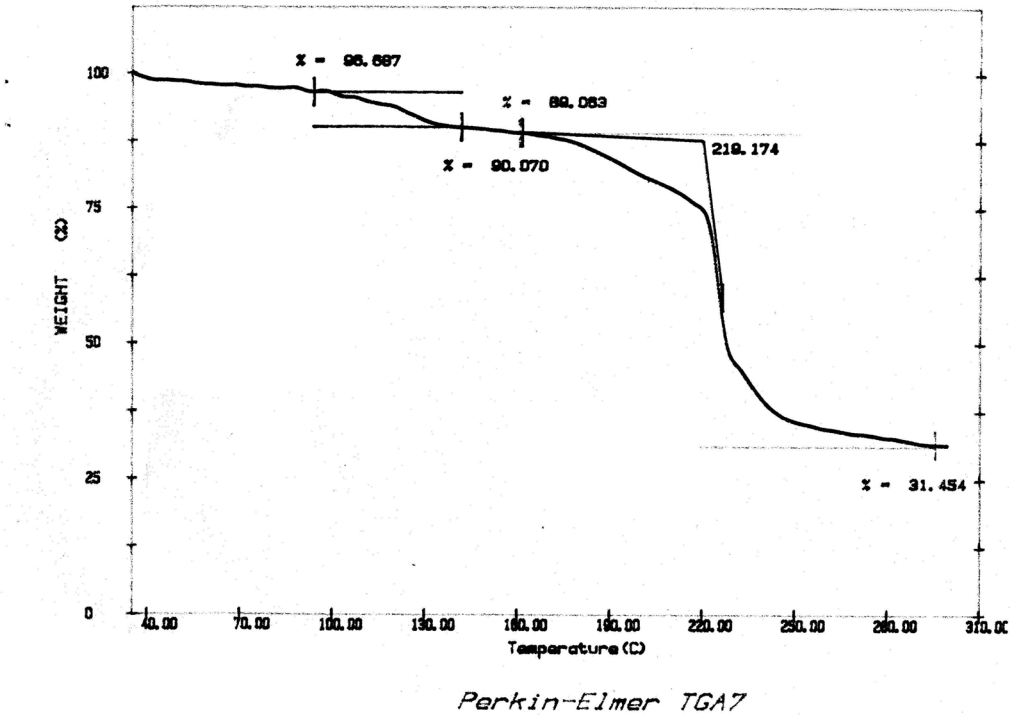

Fig. The thermogram of the complex (obtained from reaction of (*R*)-HL[1] with 93.6% ee, *L*-DBTA·H_2O and $Cu(OAc)_2 \cdot H_2O$ (1:1:2 molar ratio) in acetonitrile).

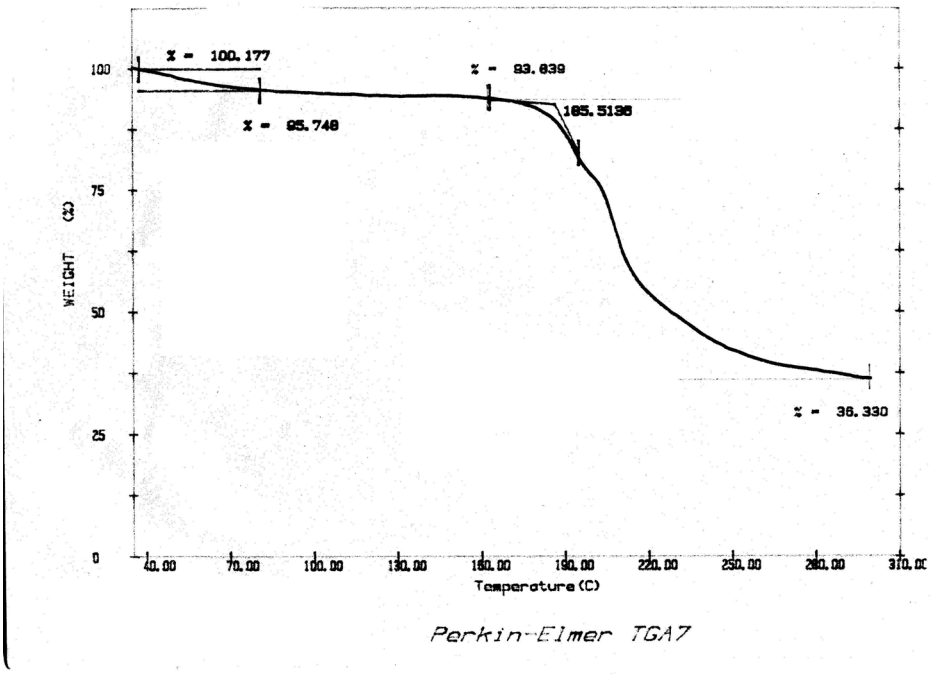

Fig. The thermogram of the complex (obtained from the reaction of (*R*)-HL[1] with 93.3% ee, *D*-DBTA·H_2O and $Cu(OAc)_2 \cdot H_2O$ (1:1:2 molar ratio) in EtOH/H_2O (v/v, 3:1)).

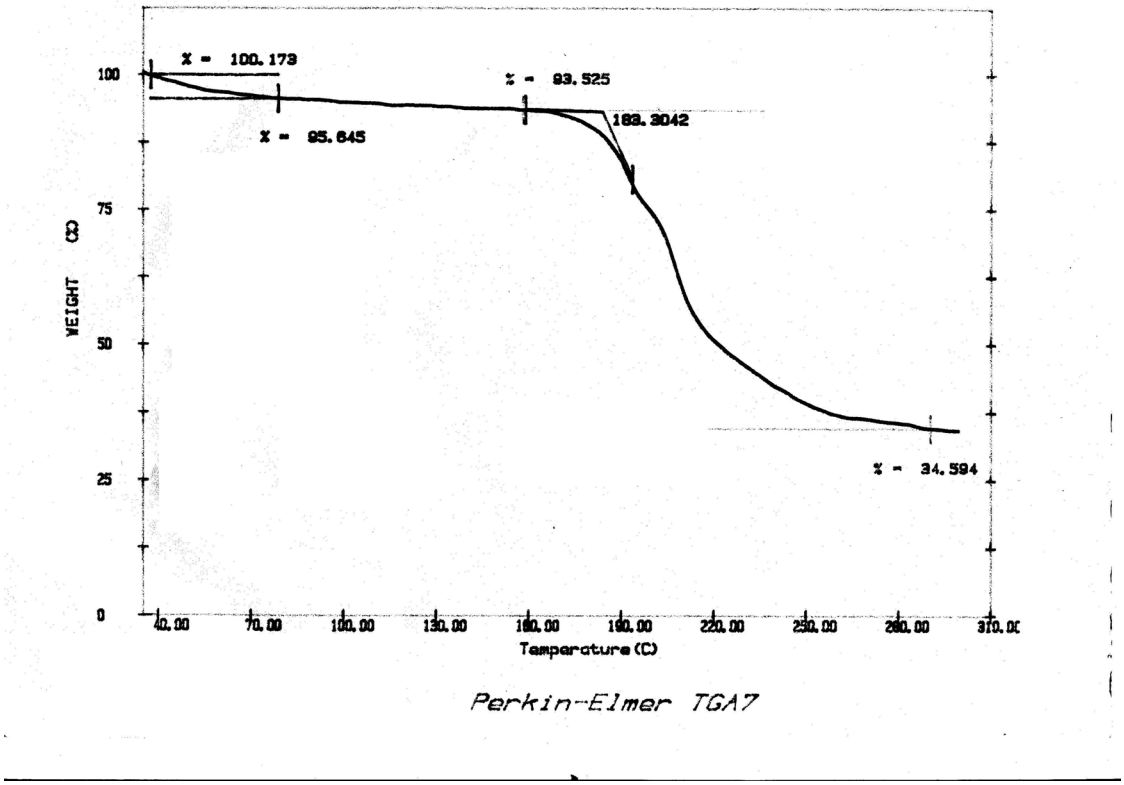

Fig. The thermogram of the complex (obtained from the reaction of (*R*)-HL[1] with 93.3% ee, *L*-DBTA·H_2O and $Cu(OAc)_2 \cdot H_2O$ (1:1:2 molar ratio) in EtOH/H_2O (v/v, 3:1).